Predictive Control of Traveling Wave Ultrasonic Motors using Neural Network

Mohammadreza Ahmadi, Hamed Mojallali, and Mohammad Hossein Fotovvati
Department of Electrical engineering
University of Guilan
Rasht, Iran
Emails: mrezaahmadi@ieee.org, mojallali@guilan.ac.ir, fotovvati.h@gmail.com

Abstract— **Traveling Wave Ultrasonic Motors (TWUSMs) possess extreme nonlinear properties such as saturation reverse effect and dead-zone, which are reliant on the driving conditions. These characteristics make modeling and control of TWUSMs highly challenging. Thus, deriving a simple and precise mathematical model suitable for controlling USMs has been a major problem for researchers. In this paper, a multi-layer perception neural network (MLPNN) based on the Hammerstein structure of TWUSMs is utilized to annul the nonlinear subsystem of TWUSM. Subsequently, a Generalized Predictive Controller (GPC), along with the inverse model characterized by MLPNN, is utilized to control the angular position of a TWUSM. The inverse model is able to cover all the variations in initial conditions, load torque, and the driving frequency. Simulation results based on the proposed scheme are presented which validate the scheme's performance.**

Keywords-Ultrasonic Motor; Neural Network; Hammerstein Model; Generalized Predictive Control

I. INTRODUCTION

Traveling wave ultrasonic motors (TWUSMs) have unique performance features such as compactness, no electromagnetic interferences, high torque at low speed, silent operation, high holding load without supply, and etc [1]. As a result, several practical applications for USMs have been suggested in literature [1].

The driving principle of USMs is established upon mechanical vibration at high frequencies and its resultant interactions with the frictional force [1]. Thus, the speed characteristics of TWUSMs have extreme nonlinear properties; thus, extracting a corresponding mathematical model is a brutal task. In addition, complicated mathematical models are not appropriate when it comes to designing a controller for TWUSMs. The analytical model has a lot of variables and is not suitable for practical applications. On the other hand, having a comprehensive model is necessary, inasmuch as TWUSM's characteristics vary with different motor variables like temperature, load torque, and the driving frequency [1].

Several research activities and investigations on the subject of modeling TWUSMs have been conducted so far. Available modeling methods are chiefly performed using equivalent circuit approaches [2], analytical schemes [3] and finite element methods (FEM) [4]. Also, black box models for TWUSMs based on Hammerstein structure were suggested in [5,6]. However, there are some serious drawbacks to these models. The method suggested in [6] is established upon "Trial and Error". The proposed algorithm in [5] depends on amplitude as the input for modeling, which is not a conventional method for controlling TWUSM. Moreover, both methods lack computational simplicity, they are significantly time consuming, and deficient in having a uniform formula for backward and forward rotation directions of TWUSM.

The main idea of this paper is upon ruling out the nonlinear part of the speed characteristics of TWUSM in order to have a simple and accurate model. Therefore, a Hammerstein model structure for TWUSM, which consists of separate nonlinear and linear subsystems, is considered. A MLPNN is proposed to act as the inverse of the nonlinear subsystem; as a consequence, the nonlinear subsystem and its corresponding inverse block (fabricated from neural networks) could cancel each other with a good estimation, leaving behind a simple dynamic first order second type linear block. The parameters of the linear subsystem are set by experimental results. Subsequently, a generalized predictive controller (GPC) is readily utilized to control the angular position and the speed of rotor.

The framework of this paper is as follows. Section II considers a concise description of the operating principles of TWUSMs. The Hammerstein model for TWUSMs and some discussions on the dead-zone effect in TWUSMs are outlined section III. In section IV, the MLPNN structure is described. Section V deals with designing an appropriate generalized predictive controller. Results based on the proposed scheme are addressed in section VI. Section VII concludes the paper.

II. OPERATING PRINCIPLES OF TWUSM

A cutaway view of a typical USR60 traveling wave ultrasonic motor is illustrated in Fig. 1, which is investigated in this study. Two major parts can be readily identified: the stator and the rotor. Vibrating with an ultrasonic frequency, the stator provokes the rotor by means of the frictional forces between them. Stator consists of a resilient body and a slight piezo-ceramic ring which is shackled below the flexible body. The ring accomplishes the task of exciting the traveling bending waves and is shown in Fig. 2. The piezo-ceramic ring is divided into two halves: phase A and phase B. Sensor and

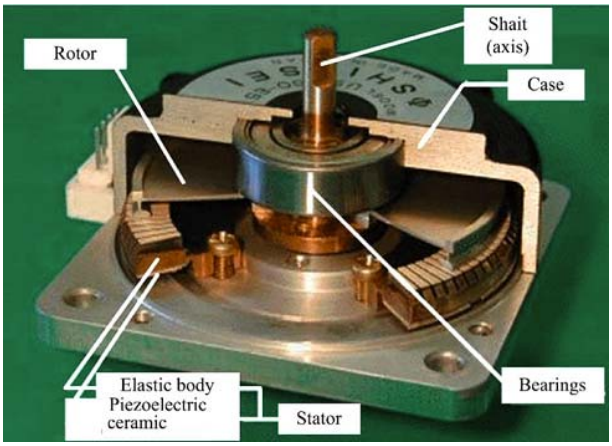

Fig. 1. The cutaway view of a Shinsei USR60 TWUSM

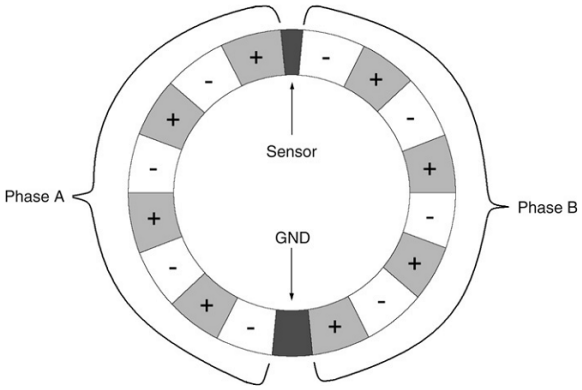

Fig. 2. The piezoceramic ring of the experimental ultrasonic motor

Table I. Rated Values of USR60

Driving Frequency	41 kHz
Rated Voltage	100 $V_{r.m.s}$
Rated Load Torque	0.32 $N.m$
Rated Output Power	3 W
Rated Speed	90 $r.p.m$
Rated Current	53 $mA \times 2 phase$
Starting Load Torque	3 $Kg.cm$
Holding Torque	3.2 $Kg.cm$
Temperature	-10 - +50 $^{\circ}C$
Weight	240 g

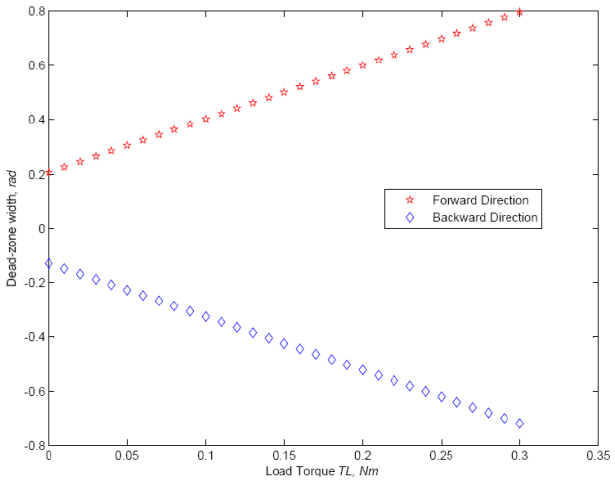

Fig. 3. The variations of the dead-zone width with load torque

ground parts, which are a quarter and 3 quarters of a wavelength respectively, separate these two phases. Each phase (A or B) includes n segments. Each segment has an opposite polarization with respect to the adjacent one and is a half wavelength of the other. The phase difference between phase A and phase B is a quarter of the wavelength. Two sinusoidal voltages which are temporally 90◦ out of phase excite the phases. Consequently, the particles on the surface of the stator swift elliptically and a traveling wave is created. To control the excitation of the piezo-ceramic ring, the amplitude and the phase of the traveling wave is measured using the sensor part. A disk spring pushes the rotor against the stator, and a thin contact layer is bonded to the rotor in the contact region. As a consequence, the small-amplitude high-frequency vibrations of the stator are converted into a lower-frequency macroscopic rotary motion of the rotor by friction. Three parameters are conventionally used for adjusting the speed of TWUSMs: the phase difference between the two-phase voltages, the frequency and the amplitude of the two-phase voltages. A comprehensive description regarding the working principles of TWUSMs is available in [1].

III. HAMMERSTEIN STRUCTURE FOR TWUSM

The Hammerstein model is comprised of a nonlinear gain function in series with a linear dynamic subsystem. In order to determine the parameters in the linear subsystem of Hammerstein model, experimental data from a USR60 motor is collected. Rated values for this specific motor are given in Table I. TWUSM exposes a dynamical behavior that can be explained by the following transfer function [7]:

$$\frac{\omega(s)}{V(s)} = \frac{k_m}{1+\tau s} \tag{1}$$

τ and k_m are the TWUSM's time constant and steady state gain, respectively. The typical values of these parameters for USR60 are 10.25 and 0.0035 sec [7]. The nonlinear subsystem is determined using the experimental data. The overall model completely confirms the practical results of USR60 and covers various conditions in driving frequency and the applied load torques. It is worth noting that the chief nonlinear behavior of USMs is the dead-zone which is dependent on load torque. The variations of the dead-zone region versus the load torque are given in Fig.3. Additionally, the fluctuations of the speed characteristics versus applied phase difference influenced by different loads are illustrated in Fig.4. Accordingly, the dead-zone width expands as the load torque increases. A Hammerstein model for TWUSM is portrayed in Fig.5.

By using phase difference as the control input, one can alter the rotation direction of the rotor or stop it smoothly by modifying the direction of the travelling wave. The driving frequency, on the other hand, makes it possible to control motor speed by the means of adjusting the ultrasonic vibration

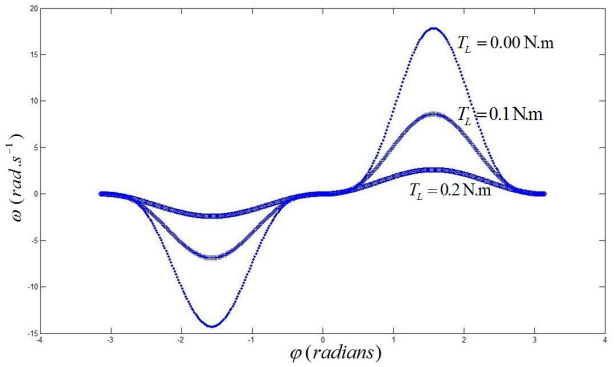

Fig. 4. Alterations of speed characteristics versus phase difference in different load torques.

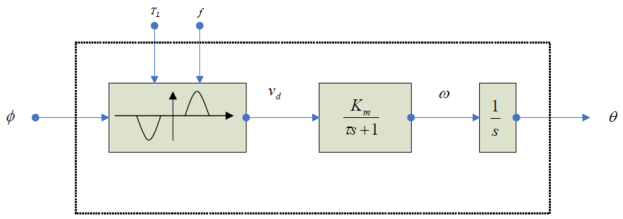

Fig. 5. A Hammerstein model for TWUSM

force. In addition, phase difference is a more prevalent control input for TWUSMs [7]. In this paper, a constant driving frequency (41 KHz) is selected, and the phase difference of the applied voltage is chosen as the control input.

IV. Neural Networks for Modeling the Inverse of the Nonlinear Subsystem

A Multi-Layer Perceptron Neural Network (MLPNN) based on back propagation learning algorithm is applied to the inputs of the nonlinear subsystem. The three-layer feed-forward MLPNN used in this study is depicted in Fig. 6. The input to the neural net and the output of the nonlinear subsystem is $v_d(k)$. The output of the neural net is current phase difference $\varphi(k)$. Cancellation occurs when the neural network is placed in the forward model, and only the linear dynamical part remains. The weights and biases of hidden layer will be updated through learning in order to decrease the error between the real and the desired position. The learning algorithm for this network is based on the Levenberg-Marquardt method which is fast, uses less memory and needs fewer neurons to get a rather precise estimation. The network is tuned to decrease the position/speed error using the back-propagation algorithm. The mathematical equations regarding the mentioned neural network are given below:

$$I_i = \sum_{j=k}^{n} \omega_{ji}\, y_j \tag{2}$$

$$y_i = f(I_i) \tag{3}$$

$$f(x) = \frac{1}{1+e^{-x}} \tag{4}$$

where I_i is the input to the ith neuron, and y_i is the output of the ith neuron. $f(*)$ signifies the activation function. Owing

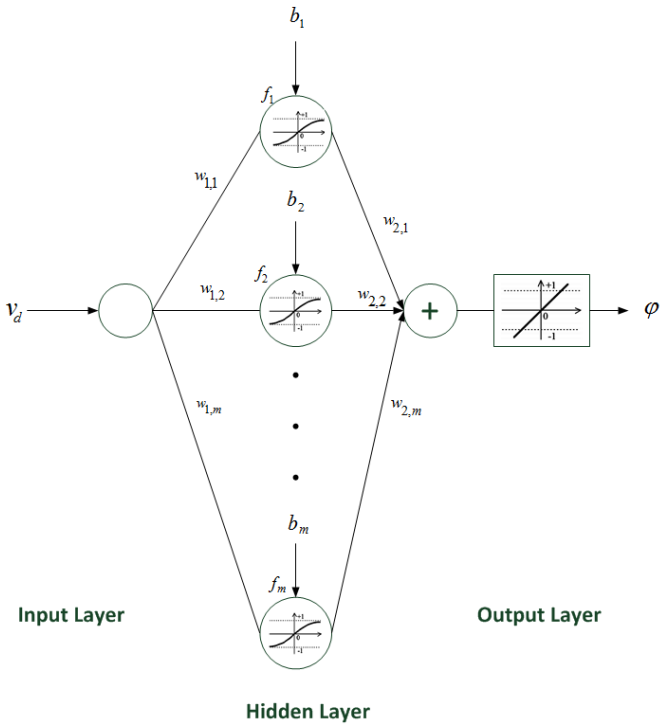

Fig. 6. The proposed three-layer MLPNN.

to the fact that the neural network controller uses input, output, and reference signals, the system acts as an adaptive proportional gain controller. The inputs are dispatched to the output layer from the hidden layer, and then the weights are updated. Updating rules are given as follows:

$$\omega_{j,i}(k) = \alpha.\omega_{j,i}(k-1) + \Delta\omega_{j,i} \tag{5}$$

$$\Delta\omega_{j,i} = \beta.E.f(I_j) \tag{6}$$

$$E^{output} = e(k) = \varphi_m(k) - \varphi(k) \tag{7}$$

$$E^{middle} = \frac{\partial f\left(I_i^{middle}\right)}{\partial I} \cdot \sum_{i=k}^{n} \left\{\omega_{j,i}.E^{output}\right\} \tag{8}$$

In which, $0 < \alpha \le 1$ is the overlearning factor, $0 < \beta \le 1$ is the learning factor which can be altered to enhance learning speed, E is the error in each layer, $\varphi_m(k)$ is the desired output from dataset, and $\varphi(k)$ is the output obtained from the neural net at the current iteration.

After the neural network is placed prior to the Hammerstein model, the nonlinear part would be cancelled. Then, a block with almost linear characteristics containing little nonlinearity, which are controllable via the proposed GPC, is left.

V. Generalized Predictive Controller for TWUSM

The GPC method first introduced by Clarke et al [8] is a prominent representative of the class of model predictive control strategies. The prediction of GPC would be reliant on both past and future control actions. Because future actuation signals are unknown, the method makes a set of adequate

assumptions about their values. Literature asserts that GPC can handle plants with variable or unknown dead time, open-loop instability, and non-minimum phase conditions. It is also able to systematically take into account real plant constraints in real-time [8]. Furthermore, GPC is not relatively sensitive to modeling errors, sensor noise, and over- or under-parameterization [8]. Thus, in this case, GPC stands as an outstanding candidate for controlling the TWUSM.

All predictive control algorithms use:

- An internal dynamic model of the process,
- A history of past control moves and
- An optimization cost function J over the prediction horizon

to calculate the optimum control moves. The optimization cost function is given by:

$$J = \sum_{j=N_1}^{N_2} [\theta_d(k+j) - \hat{\theta}(k+j)]^2 + \sum_{j=1}^{N_\varphi} \lambda(j)[\Delta\varphi(k+j-1)]^2$$
$$subject\ to\ \Delta\varphi(k+j) = 0\ \ for\ \ j = N_\varphi, N_\varphi+1, \ldots, N_2 \tag{9}$$

where $\hat{\theta}(k+j)$ denotes the predicted output, $\theta_d(k+j)$ is the modified set point, $\Delta\varphi(k)$ is the change in the control signal, N_1 and N_2 are the minimum and maximum prediction horizons, and N_φ is the control horizon. The weighting sequence $\lambda(j)$ is usually chosen constant and $\Delta = 1 - q^{-1}$ is the differencing operator. If model step response coefficients be noted by g_i, the predicted outputs are calculated using the following compact form:

$$\hat{\Theta} = G\ \Delta\Phi + \Theta_{free} \tag{10}$$

where

$$\hat{\Theta} = [\hat{\theta}(k+N_1)\quad \hat{\theta}(k+N_1+1)\quad \ldots\quad \hat{\theta}(k+N_2)]^T \tag{11}$$
$$\Delta\Phi = [\Delta\varphi(k)\quad \Delta\varphi(k+1)\quad \ldots\quad \Delta\varphi(k+N_\varphi-1)]^T \tag{12}$$
$$\Theta_{free} = [\theta_{free}(k+N_1)\quad \theta_{free}(k+N_1+1)\quad \ldots\quad \theta_{free}(k+N_2)]^T \tag{13}$$
$$G = \begin{bmatrix} g_{N_1} & 0 & \ldots & 0 \\ g_{N_1+1} & g_{N_1} & 0 & \ldots \\ \vdots & \vdots & \ddots & \ddots \\ g_{N_2} & g_{N_2-1} & \ldots & g_{N_2-N_\varphi-1} \end{bmatrix} \tag{14}$$

Notice that Θ_{free} represents those parts of the future outputs that only depend on the past inputs (the free response of the USM model). Equation (9) can be written as:

$$J = (\mathrm{G}\,\Delta\Phi + \Theta_{free} - \Theta_d)^{\mathrm{T}}(\mathrm{G}\,\Delta\Phi + \Theta_{free} - \Theta_d) + \lambda\,\Delta\Phi^{\mathrm{T}}\Delta\Phi \tag{15}$$

where

$$\Theta_d = [\theta_d(k+N_1)\quad \theta_d(k+N_1+1)\quad \ldots\quad \theta_d(k+N_2)]^T \tag{16}$$

Minimizing with respect to $\Delta\Phi$ yields:

$$\Delta\Phi(k) = K(\Theta_d - \Theta_{free}) \tag{17}$$

where K is the first row of matrix $(G^T G + \lambda I)^{-1} G^T$.

However, in the presence of constraints, another approach should be adopted for solving the optimal control problem. One avenue that researchers have followed in their attempt to handle such problems is the implementation of Iterative Quadratic Programming (IQP), which is able to minimize a quadratic objective function in the presence of linear constraints. The optimization problem is defined as follows:

$$\Delta\Phi_{\text{optimal}} = \arg\min_{\Delta\Phi}\left\{\frac{1}{2}\Delta\Phi^T H\,\Delta\Phi + D\,\Delta\Phi\right\} \tag{18}$$
$$subject\ \ to\ \ \ C\,\Delta\Phi \le d$$

The minimum of equation (15) can be found by:

$$\min_{\Delta\Phi} J = \min_{\Delta\Phi}\{\frac{1}{2}\Delta\Phi^T H\,\Delta\Phi + D\,\Delta\Phi\} \tag{19}$$

with $H = 2(G^T G + \lambda I)$, $D = -2(G^T(\Theta - \Theta_{free}))$, where I is an $(N_\varphi \times N_\varphi)$ unity matrix. The constraints defined on φ and $\Delta\Phi$ can be formulated with the following inequality:

$$\begin{bmatrix} I_{\Delta\varphi} \\ -I_{\Delta\varphi} \\ I_{N_\varphi} \\ -I_{N_\varphi} \end{bmatrix} \Delta\Phi \le \begin{bmatrix} \varphi_{\max} - I_\varphi \varphi(k-1) \\ -\varphi_{\min} + I_\varphi \varphi(k-1) \\ \Delta\varphi_{\max} \\ -\Delta\varphi_{\min} \end{bmatrix} \tag{20}$$

where I_{N_φ} and I_φ are $(N_\varphi \times N_\varphi)$ unity matrices, $I_{\Delta\varphi}$ is an $(N_\varphi \times N_\varphi)$ lower triangular unity matrix with all element equal to one, and $\Delta\varphi_{\min}$, $\Delta\varphi_{\max}$, $\varphi_{\min}$, $\varphi_{\max}$ are N_φ-vectors, with the constraints $\Delta\varphi_{\min}$, $\Delta\varphi_{\max}$, $\varphi_{\min}$, $\varphi_{\max}$ respectively. In this study, the input signal φ is confined to $[-\frac{\pi}{2}, \frac{\pi}{2}]$.

VI. Results and Discussions

The overall modeling and control scheme proposed in this paper is shown in Fig.7. Prior to designing a MLPNN, one should note that the number of neurons in the hidden layer is quite important. A large number of neurons in the hidden layer lead to a large amount of calculations for having a precise output which will consume more time, and memory. A more complicated model that is hard to control would also be an inevitable outcome.

On the contrary, less number of neurons may contribute to an inaccurate solution, but less convergence time and memory usage. Thus, a trade-off among memory usage, calculation time, and the population of neurons in the hidden layers should be taken into account beforehand. In order to further illustrate this discussion, Table II presents the results of simulations for different number of neurons in hidden layer.

All things considered, a three-layer MLP network is used with one neuron in the input layer, 12 neurons in the hidden layer and one aggregating neuron in the output layer. In the case where $\alpha = 1.00$, the value of the weights dramatically increases after the BP learning method is applied such that

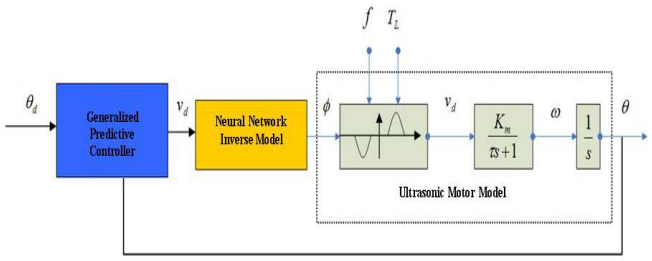

Fig. 7. The proposed control methodology

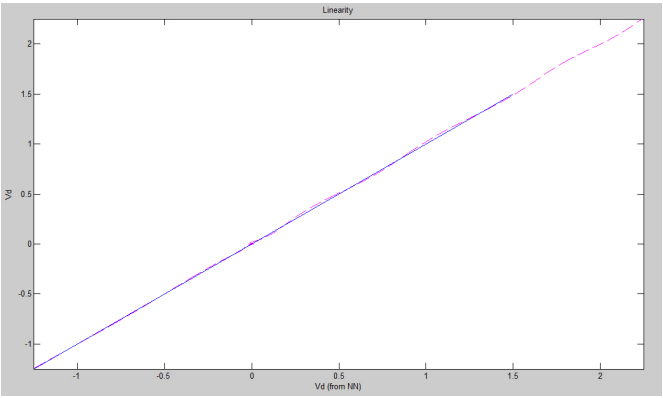

Fig. 8. The output characteristics after the cancellation in the load torque condition of 0.2 which corresponds to the maximum width of dead-zone.

rotor oscillations would occur as a result of overlearning. For a smaller value of α , similarly, the BP algorithm fails to adequately estimate the net weights. Furthermore, for large values of β , the speed error decreases rapidly; however, the control loop becomes sensible to noises. If $\beta << 1$, the algorithm for reducing the speed/position error becomes even more time consuming. Consequently, α and β should be carefully chosen to achieve an apt performance. In this study, $\alpha = 0.1$ and $\beta = 0.4$ are selected empirically in order to make a trade-off between the convergence speed and the preciseness of the speed/position control. All in all, 12 neurons in the hidden layer were chosen in this study empirically.

The activation function for the neurons in the hidden layer are chosen such that their output is limited to the span of (-1,1). Activation functions in the third layer are of a tangent-sigmoid type and a linear transfer function is selected for the neuron in the output layer.

In order to train the neural net, the input/output data set in three load conditions of (0.00, 0.1, and 0.2 N.m) were used. In all cases, the results demonstrate that the MLPNN is able to annul the nonlinear subsystem successfully. To verify the performance of the cancellation process, the output characteristics when the trained neural net is placed before the nonlinear block in the worst condition (under load torque 0.2 N.m) is shown in Fig.7. The resultant output characteristic is shown in Fig.8. So, the combination of the inverse neural model and the nonlinear subsystem results in an approximately pure linear dynamic system. Therefore, a GPC controller can cope with the model-plant mismatch and unmeasured disturbances. The estimated inverse nonlinear function and the approximation error are given in Fig.9.

Table II. Simulation results with different number of neurons

Number of neurons in hidden layer	Iteration number	Maximum error ratio %	MSE
12	504	5.22	1.04E-4
15	690	5.16	9.80E-5
20	289	5.15	9.76E-5
25	563	5.05	1.00E-4
30	369	5.13	9.98E-5

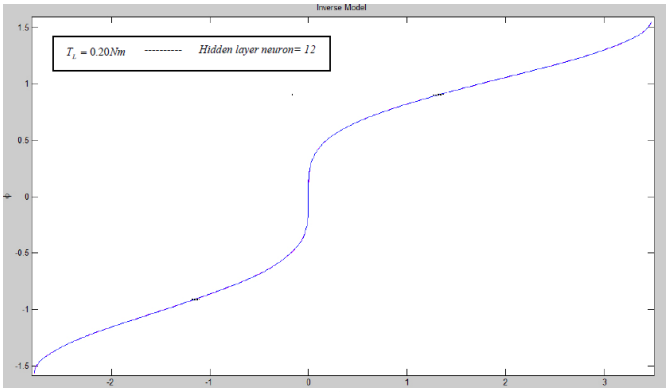

(a)

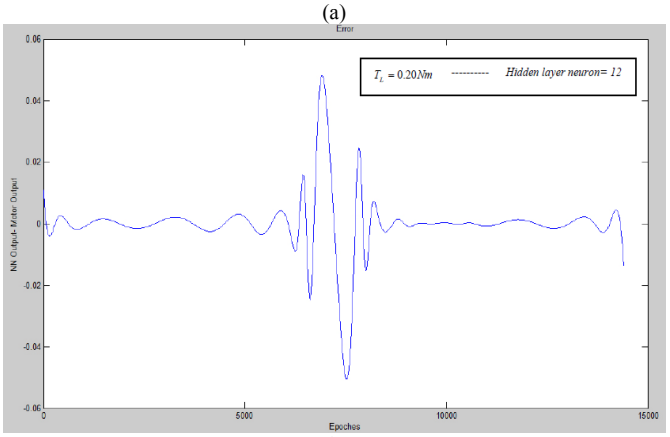

(b)

Figure 9. The approximated inverse nonlinear function (a) and the approximation error (b) using the proposed MLPNN under load torque 0.2 N m

(under load torque 0.2 N.m). The angular position signal is attained using an integrator that will be fed back to the GPC controller. The corresponding values for the control parameters are set as follows:

$$N_1 = 1,\ N_2 = 25,\ N_\varphi = 3,\ \text{and}\ \lambda = 0.1I\ .$$

Figure 10 illustrates the closed loop response for step-wise set-point under load torque 0.2 N.m. The corresponding tracking errors are given in Fig. 10, as well. As it can be seen from these figures, the proposed GPC control scheme is able to control the angular position of the rotor with quite high precision and only some trivial tracking errors exist. In all figures, the dotted plot is the ideal reference set point and the solid line is the response of TWUSM.

Table III. Results obtained using the proposed GPC.

Reference Input	Load Torque $N.m$	Iterations	Maximum error ratio %	MSE
Square Wave	0.00	58	5.31	5.62E-5
	0.01	215	7.38	9.84E-5
	0.02	586	4.86	4.86E-5
Sine Wave	0.00	21	5.31	1.06E-5
	0.01	349	7.36	1.07E-5
	0.02	545	4.91	1.07E-5

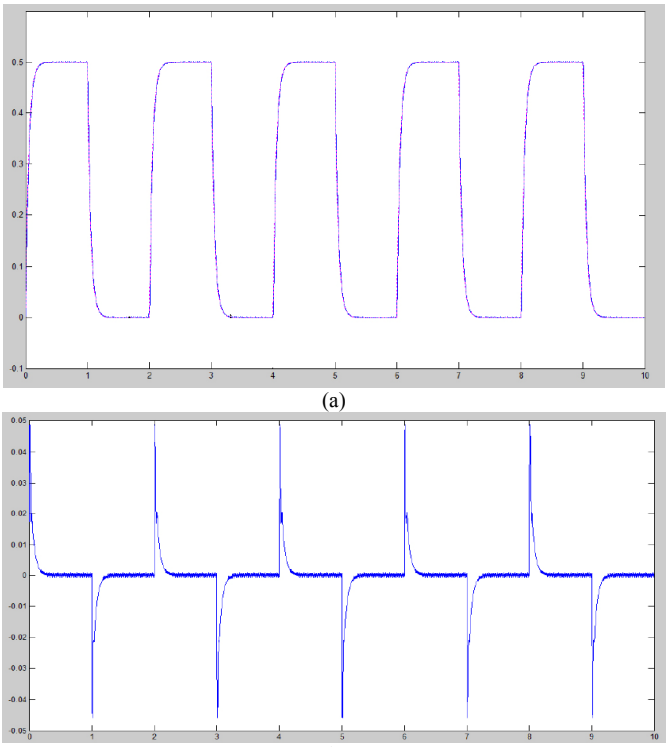

(a)

(b)

Fig. 10. Results of angular position control via the proposed GPC.

For evaluation purposes, Table III addresses an overview of errors resulted from the GPC scheme for square and sinusoidal reference input waves under different load torques. One of the most important problems in control task is load disturbance rejection. Figure 11 indicates the improved performance of disturbance rejection for periodic step-wise load torque. (In Figs. 10-11 the vertical and horizontal lines indicate the amplitude and the simulation time, respectively.)

VII. CONCLUSIONS

This paper addresses the modeling and controlling of TWUSM by means of a MLPNN and a generalized predictive controller. At first, a Hammerstein model for TWUSMs is

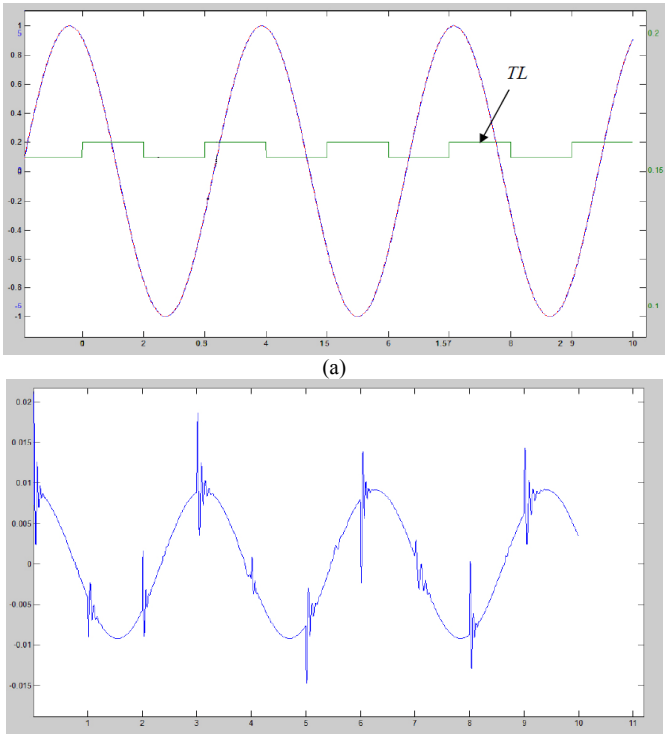

(a)

(b)

Figure 11. Disturbance rejection for sinusoidal setpoint with periodic stepwise-pulse load torque. Rotor position and disturbance signal (a) and the tracking error (b).

considered. Then, using an MLPNN the inverse of the nonlinear subsystem in the Hammerstein model is approximated so that the estimated block can be adopted to obliterate the nonlinear subsystem. Finally, a GPC is utilized to control the angular position of the TWUSM. Simulation results are given which demonstrate the proposed scheme's performance.

REFERENCES

[1] K. Uchino, "Piezoelectric Ultrasonic Motors: Overview", *Smart Materials and Structures*, vol. 7, no. 3, pp. 273-285, 1998.

[2] H. Mojallali, R. Amini, R. Izadi-Zamanabadi, A.A. Jalali, "Systematic Modeling for Free Stators of Rotary Piezoelectric Ultrasonic Motors", *IEEE/ASME Trans. Mechatronics*,vol. 12, no. 2, pp. 219-223, 2007.

[3] M. Zhou, "Contact analysis and mathematical modeling of traveling wave ultrasonic motor", *IEEE Trans. Ultrason., Ferroelect. , Freq. Control,* vol. 51, no. 6, pp. 668–79, 2004.

[4] A. Frangi, A. Corigliano, M. Binci, P. Faure, "Finite element modelling of a rotating piezoelectric ultrasonic motor", *Ultrasonics*, vol. 49, no. 9, pp. 747–755, 2005.

[5] X.L. Zhang, Y.H. Tan, "Modeling of Ultrasonic Motor with Dead-zone Based on Hammerstein Model Structure", *JZUS*, vol. 9, no. 1, pp. 58-68, 2008.

[6] N. Bigdeli, M. Haeri, "Modeling of an Ultrasonic Motor Based on Hammerstein Model Structure", Proc. Int. Conf. on Control, Automation, Robotics and Vision, pp. 1374-1378, 2004.

[7] T. Senjyu, T. Kashiwagi, K. Uezato, "Position control of ultrasonic motors using MRAC with dead-zone compensation", *IEEE Trans. Ind. Electron,* vol. 48, no. 6, pp. 1278-85, 2001.

[8] D.W. Clarke, C. Mohtadi, P.S. Tuffs, "Generalized Predictive Control-Part 1. The Basic Algorithm, *Automatica,* vol. 23, no. 2, pp. 137-148, 1987.